Supporting Information

Stable Layered Ni-rich $LiNi_{0.9}Co_{0.07}Al_{0.03}O_2$ Microspheres Assembled with Nanoparticles as High Performance Cathode Material for Lithium-Ion Batteries

*Pengfei Zhou, Huanju Meng, Zhen Zhang, Chengcheng Chen, Yanying Lu, Jun Cao, Fangyi Cheng, and Jun Chen**

Table S1. The comparison of electrochemical performance between reported LNCA materials and $LiNi_{0.9}Co_{0.07}Al_{0.03}O_2$ in this work.

Composition	1st discharge capacity at 0.1C (mA h g^{-1})	Cycling capacity at 25 °C (mA h g^{-1})				Rate capacity (C, mA h g^{-1})			Elevated temperature cycling capacity			
		current density (mA g^{-1})	cycle number	reversible capacity	capacity retention	1	5	10	temperature (°C)	cycling capacity (mA h g^{-1}) current density	cycling capacity (mA h g^{-1}) Cycle number	cycling capacity (mA h g^{-1}) capacity retention
$LiNi_{0.8}Co_{0.15}Al_{0.05}O_2$[1]	218	180	100	168	93%	172	137	115	55	180	100	72%
$LiNi_{0.8}Co_{0.15}Al_{0.05}O_2$[2]	203.1	180	200	160.3	93.3%	171.8	N/A	N/A	N/A	N/A	N/A	N/A
$LiNi_{0.8}Co_{0.15}Al_{0.05}O_2$[3]	190	170	50	169.5	98%	173	N/A	N/A	55	170	50	80%
$LiNi_{0.81}Co_{0.10}Al_{0.09}O_2$[4]	199	200	200	147.9	85%	176	161	155	60	200	200	59%
$LiNi_{0.85}Co_{0.10}Al_{0.05}O_2$[4]	207	N/A	N/A	N/A	N/A	175	158	145	60	200	200	53%
$LiNi_{0.89}Co_{0.11}O_2$[4]	200	200	200	149.3	79%	169	148	128	60	200	200	37%
$LiNi_{0.9}Co_{0.1}O_2$[5]	218	25	15	192	88.1%	N/A	N/A	N/A	N/A	N/A	N/A	N/A
$LiNi_{0.9}Co_{0.05}(Mg,Mn)_{0.025}O_2$[6]	201.0	180	50	172.5	91.9%	187.6	N/A	N/A	N/A	N/A	N/A	N/A
$LiNi_{0.9}Co_{0.07}Al_{0.03}O_2$[this work]	236.0	180	100	179.8	93.1%	193.1	168.5	140.8	45	180	100	92.8%
		180	200	169.2	87.6%				55	180	100	83.8%
		360	200	155.3	86.3%				60	180	100	70.4%

The calcination temperature and molar ratio of Li/M (M=Ni, Co, Al) play an important role in phase structure of $LiNi_{0.9}Co_{0.07}Al_{0.03}O_2$ materials and the Ni^{2+}/Li^{+} mixing especially. Thus, the calcination temperature is firstly optimized among the 650, 700, 750, and 800 °C with molar ratio of Li/M=1.05. The sample calcined at 700 °C exhibits the highest value of *I(003)/I(104)* and better hexagonal ordering as compared to the other three samples, and possesses fine spherical particles (Fig. S1, Fig. S2, and Table

S2). Thus, the optimal calcination temperature is considered as 700 °C for this component. Furthermore, the molar ratio of Li/M is further optimized among 1.0, 1.02, 1.05, and 1.1, and calcinated at the optimal calcination temperature at 700 °C. As can be seen that the sample with Li/M=1.02 possesses the least degree of Ni^{2+}/Li^{+} mixing and integrated layered structure (Fig. S2 and Table S2). Moreover, the morphology of sample with Li/M=1.02 shows smooth surface and clear grain boundaries as compared with other three samples, implying that few of residual lithium can be observed on the surface. The chemical composition is measured by ICP-AES (Table S3). The sample with Li/M=1.02 is closed to the theoretical component of $LiNi_{0.9}Co_{0.07}Al_{0.03}O_2$. Based on the above results, the optimal Li/M is 1.02 for this component.

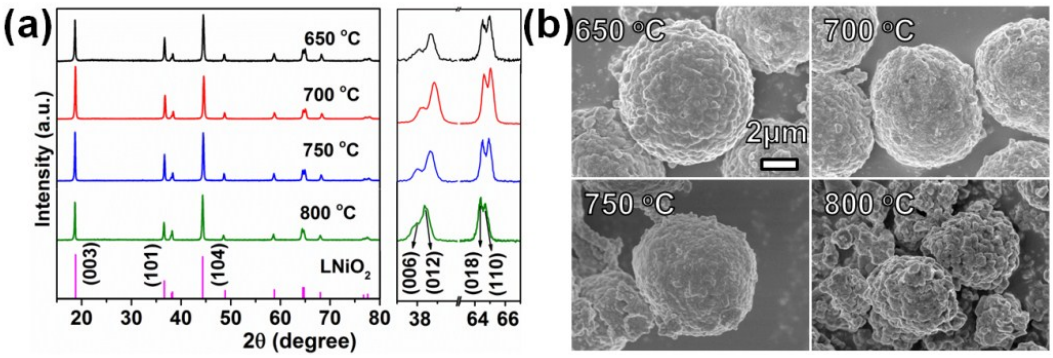

Fig. S1. (a)XRD patterns and (b) SEM images of samples with various calcination temperatures.

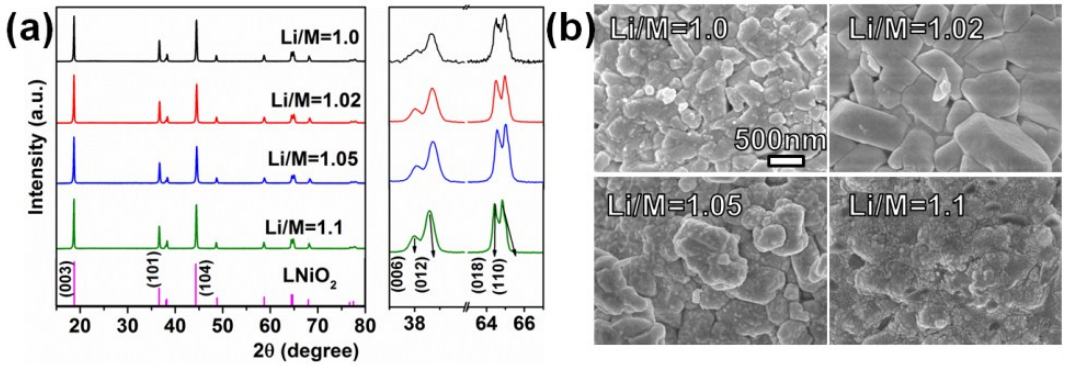

Fig. S2. (a) XRD patterns and (b) SEM images of samples with various molar ratio of Li/M.

Table S2. Structural parameters, *I(003)*/*I(104)*, and R-factor of samples synthesized under different reaction conditions

	Li/M=1.05				700 °C		
	650°C	700°C	750°C	800°C	Li/M=1.0	Li/M=1.02	Li/M=1.1
a (Å)	2.870(4)	2.874(9)	2.870(7)	2.879(2)	2.873(2)	2.871(5)	2.873(6)
c(Å)	14.175(9)	14.212(4)	14.189(9)	14.199(5)	14.190(5)	14.214(5)	14.195(1)
I(003)/ *I(104)*	0.91	1.22	1.08	0.84	1.1	1.26	1.13
R-factor	0.52	0.49	0.46	0.67	0.51	0.44	0.53

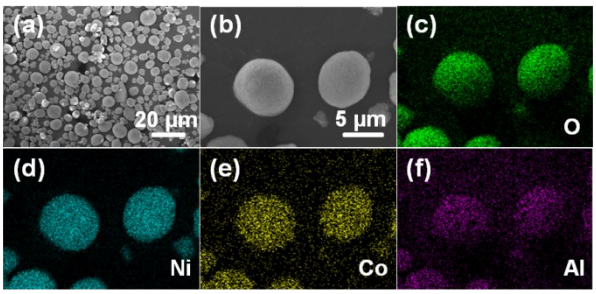

(g)

	Molar ratio		
	Ni	Co	Al
ICP	0.9037	0.0671	0.0292
Theoretical value	0.9	0.07	0.03

Fig. S3. a,b) SEM images, c-f) EDS mappings, and g) atomic ratio of Ni, Co, and Al of the as-prepared $Ni_{0.9}Co_{0.07}Al_{0.03}(OH)_2$ precursor.

Table S3. Chemical composition analysis of samples with various molar ratio of Li/M.

Composition	Molar ratio			
	Li	Ni	Co	Al
Li/M=1.0	0.976	0.9033	0.0674	0.0293
Li/M=1.02	1.009	0.9030	0.0675	0.0295
Li/M=1.05	1.034	0.9035	0.0671	0.0294
Li/M=1.1	1.085	0.9030	0.0673	0.0297

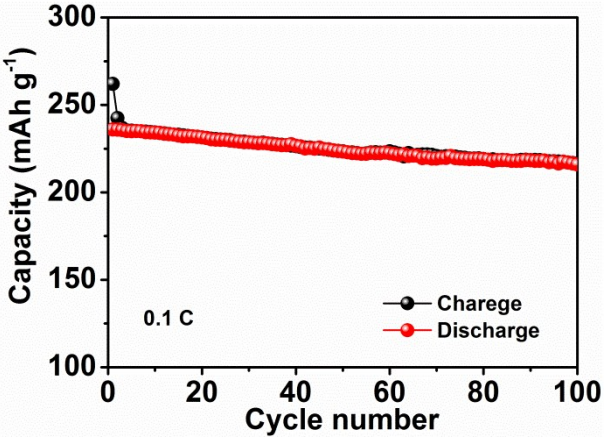

Fig. S4. Electrochemical performance of $LiNi_{0.9}Co_{0.07}Al_{0.03}O_2$ at 0.1 C for 100 cycles.

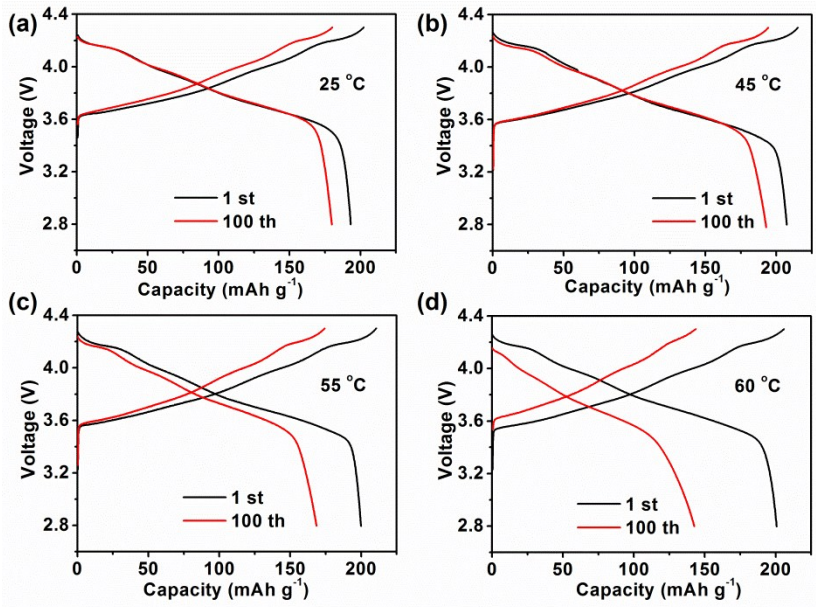

Fig. S5. Charge and discharge profiles at selected cycles at a rate of 1 C at various temperature.

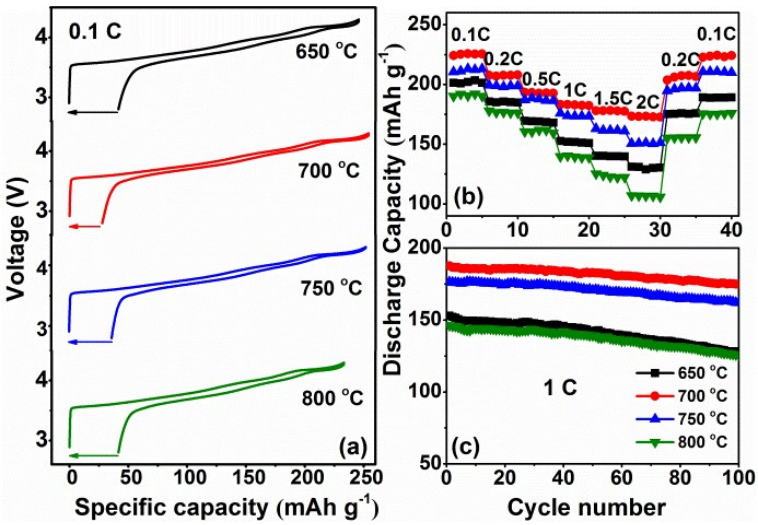

Fig. S6. Electrochemical performance of samples at various calcination temperatures.

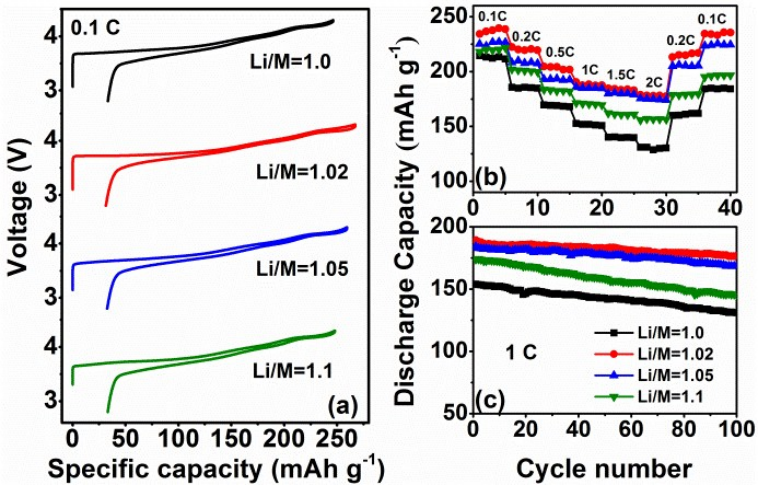

Fig. S7. Electrochemical performance of samples at various molar ratios of Li/M.

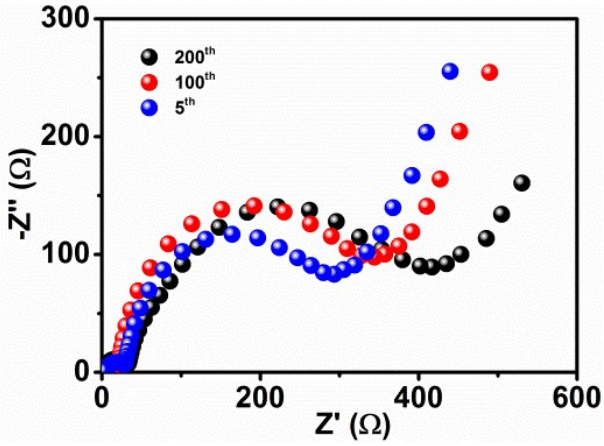

Fig. S8. Electrochemical impedance spectra of $LiNi_{0.9}Co_{0.07}Al_{0.03}O_2$ at selected cycles at a rate of 1 C at 25 °C.

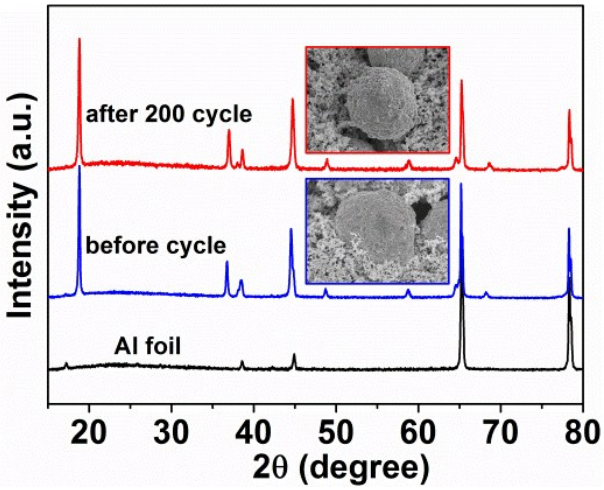

Fig. S9. XRD patterns and SEM images (inset) of $LiNi_{0.9}Co_{0.07}Al_{0.03}O_2$ before cycle and after 200 cycles at a rate of 2 C.

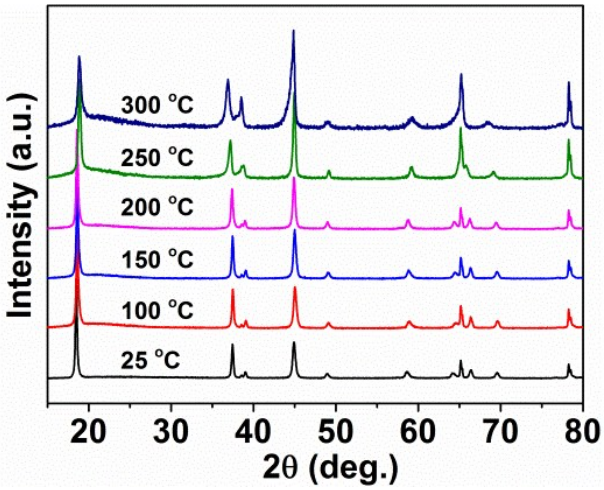

Fig. S10. Ex-situ XRD patterns of $LiNi_{0.9}Co_{0.07}Al_{0.03}O_2$ charged at 4.3 V before and after heating at various temperatures.

GITT test: The GITT curves in rage of 2.8-4.3 V at a current density of 0.1 C at the third cycle are shown in Fig. S11. The cell is charged for 10 min followed by a relaxation time interval of 40 min, and this procedure is repeated until the voltage reached to 4.3 V. A typical GITT titration step at around 3.85 V with labeling parameters is presented as Fig. S12. Based on Fick's second law of diffusion and followed assumption and simplification, the D_{Li^+} can be calculated by the simplified Equation (1).[7]

$$D_{Li^+} = \frac{4}{\pi}\left(\frac{m_B V_M}{M_B A}\right)^2\left(\frac{\Delta E_S}{\tau(dE_\tau/d\sqrt{\tau})}\right)^2 \qquad (\tau \ll L^2/D_{Li^+}) \qquad (1)$$

where m_B and M_B are the mass and molecular weight of $LiNi_{0.9}Co_{0.07}Al_{0.03}O_2$ cathode material, respectively. V_M, the molar volume of $LiNi_{0.9}Co_{0.07}Al_{0.03}O_2$, is calculated from the crystal structure data and equal to $(N_A \times V_{unit})/3$, where N_A is Avogadro constant, and V_{unit} is the volume of unit cell. A is the total contact area between the cathode material and electrolyte. L is the average thickness of the electrode. Detailed definition of τ, ΔE_S, and ΔE_τ is demonstrated in Fig. S10. Furthermore, when the cell voltage during titration is linearly proportional to $\tau^{1/2}$ (Fig. S13), the Equation (1) can be further simplified as Equation (2). [7]

$$D_{Li^+} = \frac{4}{\pi\tau}\left(\frac{m_B V_M}{M_B A}\right)^2\left(\frac{\Delta E_S}{\Delta E_\tau}\right)^2 \qquad (2)$$

In this case, the BET surface area of the compound electrode (3.98 $m^2 g^{-1}$, Fig. S14, Supporting Information) is used as the total contact area rather than the geometric area of the electrode (0.785 cm^2), because of the electrolyte can fully soak the cathode materials by permeating the conductive additive and binder. [8]

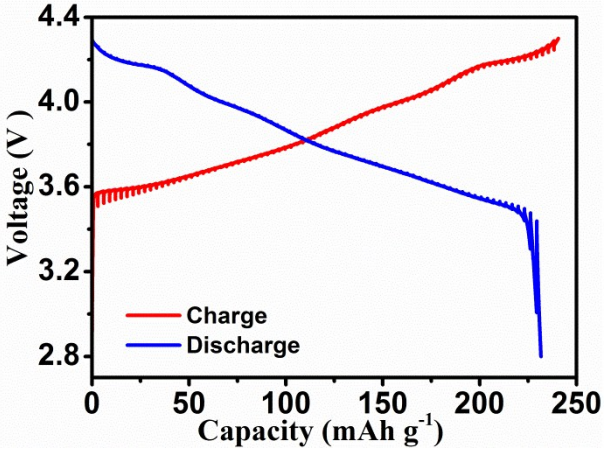

Fig. S11. The GITT curves of $LiNi_{0.9}Co_{0.07}Al_{0.03}O_2$ during the third cycle in the voltage

range of 2.8-4.3 V at a rate of 0.1 C and at 25 °C.

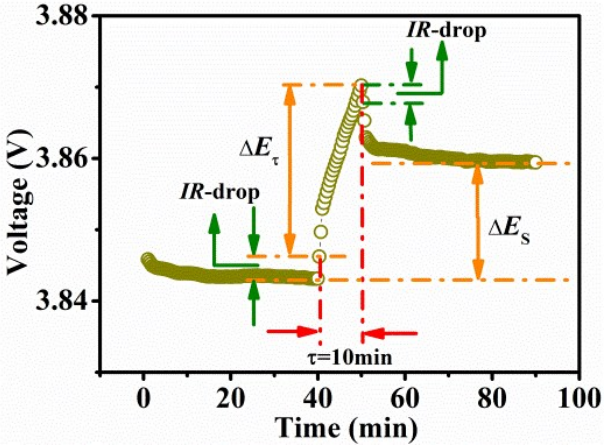

Fig. S12. Scheme for the voltage response of a charge pulse at around 3.85 V in the GITT experiment with labeling of parameters.

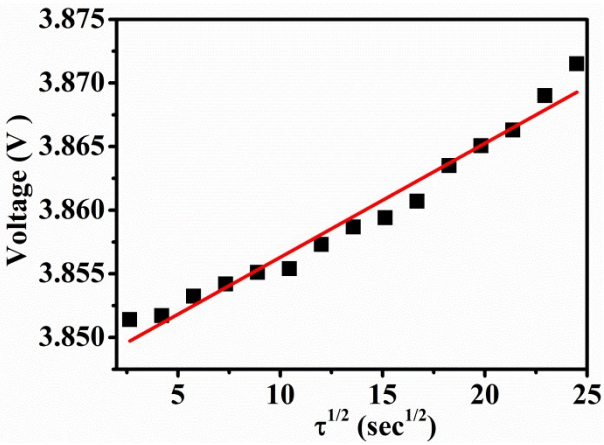

Fig. S13. Plot of voltage against $\tau^{1/2}$ to show the linear fit.

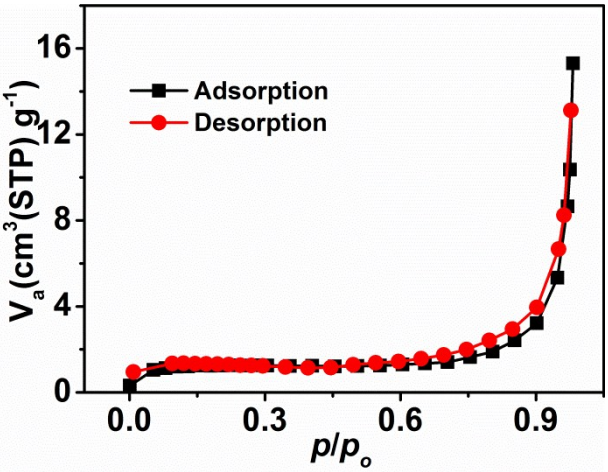

Fig. S14. N_2 adsorption and desorption isotherm of the composite electrode.

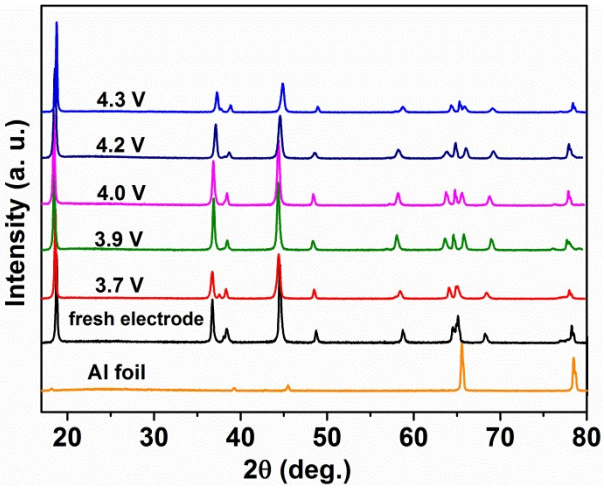

Fig. S15. Ex-situ XRD patterns of as-prepared $LiNi_{0.9}Co_{0.07}Al_{0.03}O_2$ at different charged state during the third charge process at a rate of 0.1 C and at 25 ^oC.

Table S4. The lattice patterns of $LiNi_{0.9}Co_{0.07}Al_{0.03}O_2$ at different stage of charging.

	pristine	3.7 V	3.9 V	4.0 V	4.2 V	4.2 V
a	2.8659	2.8752	2.8803	2.8905	2.8925	2.8938
c	14.2100	14.375	14.4460	14.4504	14.1929	14.1794

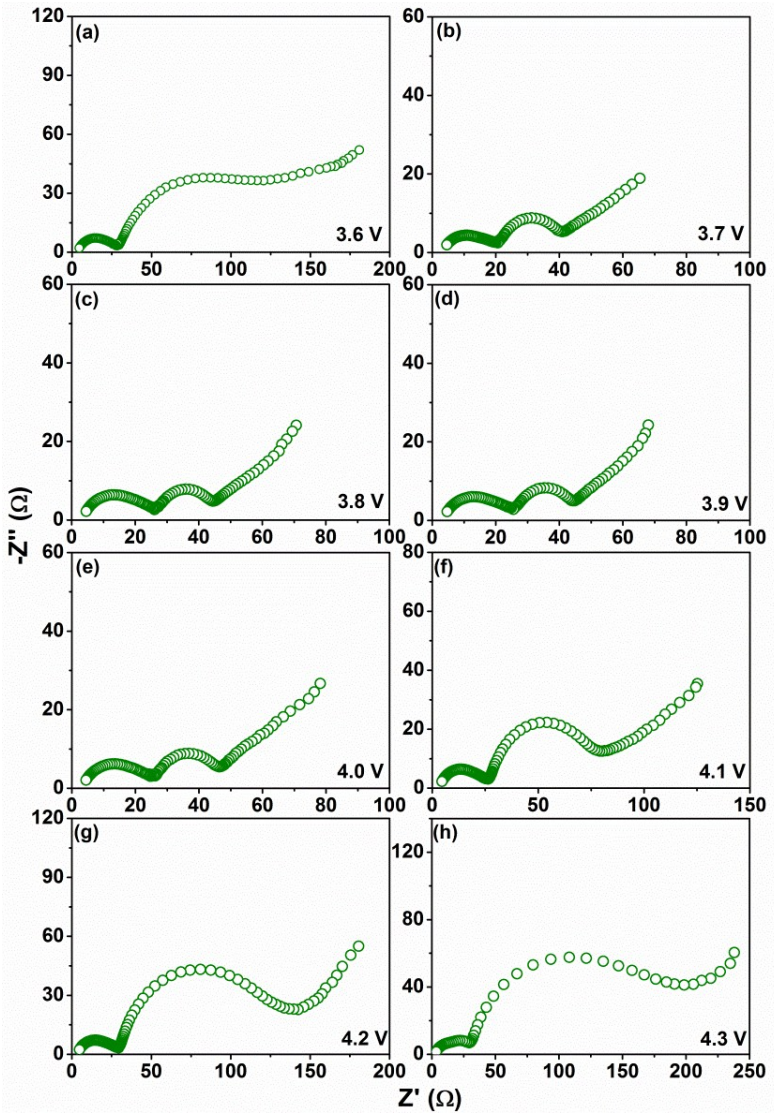

Fig. S16. EIS of $LiNi_{0.9}Co_{0.07}Al_{0.03}O_2$ at different stage of charge during the third cycle.

Table S5. The comparisons of lithium and electronic conductivity between the reported Ni-based cathode materials and as-prepared $LiNi_{0.9}Co_{0.07}Al_{0.03}O_2$.

	Morphology	Type of electrode	D_{Li^+} ($cm^2\ s^{-1}$)	electron conductivity ($S\ cm^{-1}$)	Technique used for test D_{Li^+}
$LiNi_{0.8}Co_{0.15}Al_{0.05}O_2$[1]	microrods	composite	$3.89\cdot10^{-10}$	N/A	EIS
$LiNi_{0.8}Co_{0.15}Al_{0.05}O_2$[1]	spherical	composite	$3.72\cdot10^{-11}$	N/A	EIS
$LiNi_{0.8}Co_{0.15}Al_{0.05}O_2$[3]	spherical	composite	$8.3\pm0.9\cdot10^{-16}$	N/A	EIS
$LiNi_{0.8}Co_{0.15}Al_{0.05}O_2$[9]	spherical	composite	$\sim10^{-11}$	N/A	EIS
			$\sim3\cdot10^{-11}$		AC
$LiNi_{0.8}Co_{0.15}Al_{0.05}O_2$[10]	spherical	pure NCA	$\sim2\cdot10^{-11}$	$\sim10^{-4}$	DC
			$\sim4\cdot10^{-11}$		Depolarization
$LiNi_{0.9}Co_{0.07}Al_{0.03}O_2$[this work]	spherical	composite	$\sim7\cdot10^{-10}$	$\sim5.4\cdot10^{-4}$	GITT

LIBs full cells

The conductive graphite (KS_6) anode was prepared by blending 90 wt% KS6 active materials and 10 wt% PVdF as the binder in N-methyl-2-pyrrolidone. The obtained slurry was pasted onto copper foil and dried at 80 ^oC for 12 h in vacuum. The anode was cut into pellets with the diameter of 12 mm. Then, the electrode pellets were tried to press under various pressure (0, 5, 10, and 15 MPa) for 5 s so as to achieve better performance. Fig. S17 shows that when pressed under 10 MPa, the KS_6 exhibited the best electrochemical performance. For full-cell demonstration, KS_6 anode was precycled in half-cells between 0.01 to 1.0 V and dissembled at charge state, then reassembled with fresh $LiNi_{0.9}Co_{0.07}Al_{0.03}O_2$ cathode into full-cells. The ratio of $LiNi_{0.9}Co_{0.07}Al_{0.03}O_2$/ KS_6 is about ~1.8.

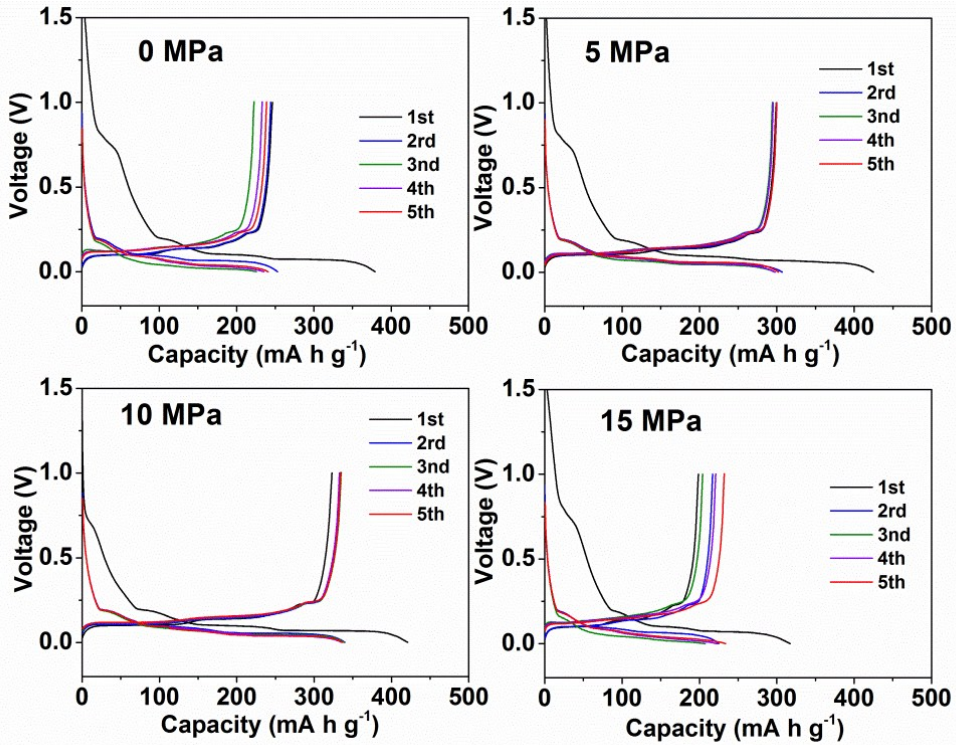

Fig. S17. Charge and discharge profiles of KS_6 in half-cells under various pressures and at current density of 18 mA g^{-1}.

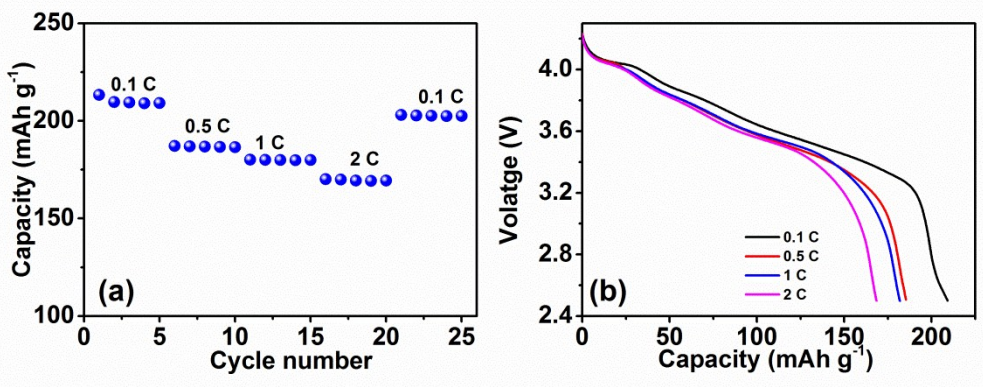

Fig. S18. (a) rate performance and (b) charge and discharge profiles at various rates of $LiNi_{0.9}Co_{0.07}Al_{0.03}O_2/KS_6$ full cell.

[1] N. T. Wu, H. Wu, W. Yuan, S. J. Liu, J. Y. Liao, Y. Zhang, *J. Mater. Chem. A,* **2015**, *3*, 13648.

[2] H. B. Xie, K. Du, G. R. Hu, J. G. Duan, Z. D. Peng, Z. Z. Zhang, Y. B. Cao, *J. Mater. Chem. A,* **2015**, *3*, 20236.

[3] T.J. Park, J. B. Lim, J.T. Son, *Bull. Korean Chem. Soc.,* **2014**, *35*, 357.

[4] M. Jo, M. Noh, P. Oh, Y. Kim, J. Cho, *Adv. Energy Mater.,* **2014**, *4*, 1301583.

[5] C.W. Wang, X.L. Ma, J.G. Cheng, X.Y. Cao, J.T. Sun, Y.H. Zhou, *Mater. Lett.,* **2007**, *61*, 556.

[6] D.C. Jiang, L. Zhao, Y.B. Shao, D.L. Wang, *RSC Adv.,* **2015**, *5*, 40779.

[7] X. H. Rui, N. Yesibolati, S. R. Li, C. C. Yuan, C. H. Chen, *Solid State Ionics,* **2011**, *187*, 58.

[8] J.M. Zheng, W. Shi, M. Gu, J. Xiao, P.J. Zuo, C.M. Wang, J.G. Zhang, *J. Electrochem. Soc.,* **2013**, *160*, A2212.

[9] D.P. Abraham, S. Kawauchi, D.W. Dees, *Electrochim. Acta,* **2008**, *53*, 2121.

[10] R. Amin, D.B. Ravnsbæk, Y.M. Chiang, *J. Electrochem. Soc.,* **2015**, *162*, A1163.